

RESEARCH ARTICLE | *Sensory Processing*

# Analysis of excitatory and inhibitory neuron types in the inferior colliculus based on $I_h$ properties

 Victor Naumov,<sup>1</sup> Julia Heyd,<sup>1</sup> Fauve de Arnal,<sup>1</sup> and Ursula Koch<sup>1,2</sup>

<sup>1</sup>Institute of Biology, Neurophysiology, Freie Universität Berlin, Berlin, Germany; and <sup>2</sup>NeuroCure Cluster of Excellence, Charité Universitätsmedizin, Berlin, Germany

Submitted 3 September 2018; accepted in final form 27 March 2019

**Naumov V, Heyd J, de Arnal F, Koch U.** Analysis of excitatory and inhibitory neuron types in the inferior colliculus based on  $I_h$  properties. *J Neurophysiol* 121: 2126–2139, 2019. First published April 3, 2019; doi:10.1152/jn.00594.2018.—The inferior colliculus (IC) is a large midbrain nucleus that integrates inputs from many auditory brainstem and cortical structures. Despite its prominent role in auditory processing, the various cell types and their connections within the IC are not well characterized. To further separate GABAergic and non-GABAergic neuron types according to their physiological properties, we used a mouse model that expresses channelrhodopsin and enhanced yellow fluorescent protein in all GABAergic neurons and allows identification of GABAergic cells by light stimulation. Neuron types were classified upon electrophysiological measurements of the hyperpolarizing-activated current ( $I_h$ ) in acute brain slices of young adult mice. All GABAergic neurons from our sample displayed slow-activating  $I_h$  with moderate amplitudes, whereas a subset of excitatory neurons showed fast-activating  $I_h$  with large amplitudes. This is in agreement with our finding that immunoreactivity against the fast-gating hyperpolarization-activated and cyclic-nucleotide-gated 1 (HCN1) channel was present around excitatory neurons, whereas the slow-gating HCN4 channel was found perisomatically around most inhibitory neurons.  $I_h$  properties and neurotransmitter types were correlated with firing patterns to depolarizing current pulses. All GABAergic neurons displayed adapting firing patterns very similar to the majority of glutamatergic neurons. About 15% of the glutamatergic neurons showed an onset spiking pattern, always in combination with large and fast  $I_h$ . We conclude that HCN channel subtypes are differentially distributed in IC neuron types and correlate with neurotransmitter type and firing pattern. In contrast to many other brain regions, membrane properties and firing patterns were similar in GABAergic neurons and about one-third of the excitatory neurons.

**NEW & NOTEWORTHY** Neuron types in the central nucleus of the auditory midbrain are not well characterized regarding their transmitter type, ion channel composition, and firing pattern. The present study shows that GABAergic neurons have slowly activating hyperpolarizing-activated current ( $I_h$ ) and an adaptive firing pattern whereas at least four types of glutamatergic neurons exist regarding their  $I_h$  properties and firing patterns. Many of the glutamatergic neurons were almost indistinguishable from the GABAergic neurons regarding  $I_h$  properties and firing pattern.

auditory midbrain; GABA; glutamate; HCN channels;  $I_h$ ; inferior colliculus

## INTRODUCTION

The inferior colliculus (IC) is a major auditory integration center where ascending projections from the auditory brainstem and descending projections from auditory cortical and subcortical areas converge (Oliver 2000). In addition, IC neurons receive prominent inputs from other excitatory and inhibitory neurons within the IC and the contralateral IC, both of them contributing to the processing of auditory information (Grimsley et al. 2013; Ito et al. 2016; Sturm et al. 2014). GABAergic neurons constitute up to 30% of all neurons in the IC (Beebe et al. 2016; Ito et al. 2009; Merchán et al. 2005), with the remaining 70% of neurons being glutamatergic (Ito et al. 2011). Previous studies identified a number of different neuron types in response to hyper- and depolarizing current injections in GABAergic and glutamatergic neurons (Ono et al. 2005), whereas response patterns to acoustic stimulation were not different between GABAergic and glutamatergic neurons (Ono et al. 2017). We were interested to what extent differences in the maturity of neurons contributed to this observed discrepancy and whether the hyperpolarization-activated and cyclic-nucleotide-gated (HCN) channel was differentially distributed among different IC neuron types.

In addition to the specific pattern of hyperpolarizing and depolarizing inputs, also voltage-gated ion channels determine the integrative properties of the neurons and their output spike pattern. HCN channels are highly expressed in auditory brainstem neurons and largely contribute to the specific integration of inputs in the ascending auditory pathway (Khurana et al. 2012; Koch and Grothe 2003). HCN channels open upon hyperpolarization and are permeable to  $K^+$  and  $Na^+$  ions. Functionally, activation of the hyperpolarization-activated current ( $I_h$ ) stabilizes the resting membrane potential, decreases the membrane time constant at rest, and reduces temporal summation of synaptic inputs (Koch and Grothe 2003; Shah 2018; Wahl-Schott and Biel 2009). Four different subunits of the HCN channel exist, namely HCN1–4, which differ in their activation time constants, their voltage-dependence, and their sensitivity to modulation by cAMP (Wahl-Schott and Biel 2009). Previous studies have shown that IC neurons express

Address for reprint requests and other correspondence: U. Koch, Freie Univ. Berlin, Institut für Biologie, AG Neurophysiologie, Takustraße 6, 14195 Berlin (e-mail: ursula.koch@fu-berlin.de).

different HCN subunits (Koch et al. 2004; Notomi and Shigemoto 2004) and display diverse  $I_h$  properties that are, in many cases, correlated with the firing patterns elicited by depolarizing current injections (Koch and Grothe 2003; Ono et al. 2005; Tan et al. 2007).

To systematically correlate  $I_h$  properties and firing pattern of mature GABAergic and non-GABAergic IC neurons, we used electrophysiological recordings in acute brain slices of a transgenic mouse model that expresses channelrhodopsin 2 (ChR2) and enhanced yellow fluorescent protein (EYFP) under the promoter of the vesicular GABA transporter (VGAT) (Zhao et al. 2011). This mouse model allows the unambiguous identification of GABAergic neurons by blue light activation also in deeper tissue of mature animals (Ono et al. 2016). Furthermore, we correlated  $I_h$  properties with the HCN isoform composition in GABAergic and glutamatergic neurons and systematically analyzed the spike pattern evoked by depolarizing current injections between the different cell types.

## MATERIALS AND METHODS

### Animals

All experiments were performed in accordance with the German animal welfare legislation and approved by the Landesamt für Gesundheit und Soziales (LAGESO, Berlin, Germany, T0262/12). VGAT-ChR2-EYFP line eight mouse founders were obtained from Jackson Laboratories [stock no. 014548, B6.Cg-Tg(Slc32a1-COP4\*H134R/EYFP)8Gfng/J]. This strain is hemizygous for VGAT-ChR2-YFP BAC transgene, viable, and fertile, with expression of the mhChR2::YFP fusion protein directed to GABAergic neurons by the mouse vesicular GABA transporter (VGAT or Slc32a1) promoter/enhancer regions on the BAC transgene. At postnatal days 2 and 3, expression of the mhChR2::EYFP construct was visually determined by directing a blue light beam (460–495 nm) with a specialized lamp (FS/ULS-02B2; BLS) to the mice. A yellow/green shimmer through the skull confirmed the expression of EYFP in the brain. Before the experiments, mice were housed in the animal facility, kept on a 12:12-h light-dark cycle, and had ad libitum access to standard laboratory food pellets and drinking water.

All chemicals were purchased from Sigma-Aldrich or Biotrend unless otherwise indicated.

### Slice Preparation

Patch-clamp recordings were performed from neurons in the central nucleus of inferior colliculus (CIC) of mice aged 22–28 days (male/female ratio ~1:1). The animals were decapitated under isoflurane anesthesia. Brains were removed in ice-cold oxygenated (95% O<sub>2</sub>/5% CO<sub>2</sub>) sucrose replacement solution as follows (in mM): 2.5 KCl, 1.25 NaH<sub>2</sub>PO<sub>4</sub>·H<sub>2</sub>O, 26 NaHCO<sub>3</sub>, 0.5 CaCl<sub>2</sub>, 6 MgCl<sub>2</sub>, 25 glucose, and 200 sucrose, pH 7.4). Transverse brainstem slices (200 μm) were cut with a vibratome (VT1200S; Leica Biosystems), incubated in oxygenated artificial cerebral spinal fluid (aCSF) at 32°C for 1 h, and afterwards maintained at room temperature. The aCSF used for incubation and experiments contained the following (in mM): 125 NaCl, 2.5 KCl, 1.25 NaH<sub>2</sub>PO<sub>4</sub>·H<sub>2</sub>O, 26 NaHCO<sub>3</sub>, 2 CaCl<sub>2</sub>, 1 MgCl<sub>2</sub>, and 25 glucose (pH 7.4). For recordings, slices were transferred to a recording chamber, which was perfused continuously with oxygenated aCSF at 32°C and visualized with the upright microscope (Axio Examiner.A1; Carl Zeiss) using infrared-differential interference contrast optics.

### Electrophysiology

Current- and voltage-clamp recordings were made from visually identified CIC neurons using a Multiclamp 700B amplifier (Molecular Devices). All recordings were made within the CIC. We adopted the classification of IC into external cortex (ECIC), CIC, and dorsal cortex according to the Nissl staining (Paxinos and Franklin 2012). Additionally visually identified clusters of dense EYFP-positive neurons in the ECIC and diffuse EYFP-positive neurons characteristic for the CIC helped us to differentiate between the ECIC and CIC (Ono et al. 2005). All experiments were performed at a near-physiological temperature of 32°C. Patch pipettes were pulled from borosilicate glass capillaries (BM150F-10P; BioMedical Instruments) on a DMZ Universal Puller (Zeitz Instruments). When filled with electrode solution, patch pipettes had a resistance of 2–4 MΩ. For current- and voltage-clamp recordings, the pipette solution contained the following (in mM): 125 potassium D-gluconate, 5 KCl, 10 HEPES, 1 EGTA, 2 Na<sub>2</sub>-ATP, 2 Mg-ATP, 0.3 Na-GTP, and 10 phosphocreatine disodium salt hydrate, adjusted to pH 7.25 with KOH.

To isolate  $I_h$  pharmacologically the following drugs were applied to the aCSF (in mM): 1 3,4-diaminopyridine, 10 tetraethylammonium chloride, 0.2 BaCl<sub>2</sub>·2H<sub>2</sub>O, 0.05 NiCl<sub>2</sub>, 0.1 CdCl<sub>2</sub>, 0.001 TTX, 0.01 DNQX disodium salt, 0.025 DL-AP5, 0.001 strychnine hydrochloride, and 0.01 SR-95531 hydrobromide. To retain iso-osmolarity, the concentration of NaCl in the aCSF was lowered to 115 mM.

### Data Acquisition and Statistical Analysis

Recordings were done with a MultiClamp 700B amplifier (Molecular Devices) and controlled by pClamp (Ver. 10.5.1.0, Molecular Devices). Both voltage and current signals were low-pass filtered at 10 kHz with a four-pole Bessel filter and sampled at a rate of 50 kHz. For voltage-clamp recordings, whole cell capacitance compensation was applied and series resistance (<12 MΩ) was compensated to a residual resistance of 2 MΩ. During voltage-clamp recordings, the holding potential was set to –60 mV. For current clamp recordings the bridge balance was adjusted to compensate for artifacts arising from electrode resistance.

All electrophysiological data were analyzed in Clampfit (Ver. 10.5., Molecular Devices) and IGOR Pro (Ver. 6.2., WaveMetrics) using the custom-written package Neuromatic (UCL, London, UK) and in Excel (Microsoft Office 2010). The junction potential was –10.5 mV, and was corrected during analysis.

Pharmacologically isolated  $I_h$  was activated by applying depolarizing and 1-s long hyperpolarizing voltage steps from –55.5 to –120.5 mV (step width 5 mV). Tail currents were analyzed from a 0.5-s long holding potential of –100.5 mV at the end of each voltage step.

Activation time constants of the  $I_h$  were obtained by applying a single exponential fit to the currents during hyperpolarizing voltage deflections. Current amplitudes were measured at the end of the 1-s voltage step. For neurons with slowly activating  $I_h$ ,  $I_h$  was not fully activated at this time point. However, measured taus were in any case an underestimation for slow- $I_h$  neurons and therefore did not change differences between the groups. Current density was calculated by dividing the current amplitude by the neuron's capacitance as measured during the capacitance compensation procedure. Half-maximal activation of  $I_h$  was computed from tail currents. Tail current amplitudes were determined at a holding potential of –90 mV ~20 ms after the termination of the depolarizing and hyperpolarizing voltage steps. For each neuron, amplitudes were normalized to the maximal and minimal amplitude  $[(I - I_{\min})/(I_{\max} - I_{\min})]$ . Values were fitted with a Boltzmann function to obtain the half-maximal activation voltage ( $V_{1/2}$ ).

Membrane and firing properties were characterized by hyper- and depolarizing the neurons with rectangular current pulses (duration: 500 ms; step increment: 50 pA). Input resistance was assessed from

the steady state of the hyperpolarization triggered by a  $-50$ -pA current injection according to Ohm's law. Membrane time constants were calculated from the voltage deflection in response to  $-50$ -pA current injection using a single exponential fit.

To estimate  $I_h$  properties in current clamp mode, a single exponential fit was applied to the  $I_h$  induced depolarizing sag for a  $-200$ -pA current injection. Furthermore, to estimate the amplitude of  $I_h$  activation the amplitude of the depolarizing voltage sag ( $V_{max} - V_{ss}$ ) was divided by the maximal voltage deflection ( $V_{max}$ ) during a  $-200$ -pA current pulse according to:

$$\text{Relative } V_{sag} = (V_{max} - V_{ss})/V_{max} \times 100\%$$

Neurons were divided into two categories according to their firing pattern: onset and adapting firing. As onset we declared neurons that fired one to three action potentials for current injections up to 250 pA above firing threshold. All other neurons were declared as adapting firing neurons.

The number of neurons with rebound spike was obtained for hyperpolarizations around  $-90.5$  mV at steady-state activation, a value that is close to the reversal potential of inhibitory synapses.

Mean firing frequency was calculated for bin width of 50 ms for the depolarizing current injection that elicited firing rates of  $\sim 100$  Hz in adapting firing neurons neuron. One VGAT positive (VGAT+) and eight VGAT negative (VGAT-) neurons that had maximal firing rates  $< 75$  Hz were excluded from the analysis. To quantify adaptation we used the following method: due to low spike numbers, the fitting of single and double exponential functions to the binned frequency plots was not satisfactory. Therefore the firing frequency between the first spike and each successive spike was calculated and plotted against the time point of each successive spike. Subsequently, a double exponential function  $f(t) = A_1 \exp(-t/\tau_{fast}) + A_2 \exp(-t/\tau_{slow})$  was fit to the successive spike frequency plot of each neuron. Weighted time constants ( $\tau_s$ ) were calculated for each neuron according to  $\tau_{weighted} = (A_1 \times \tau_{fast} + A_2 \times \tau_{slow})/(A_1 + A_2)$ .

Results are expressed as means  $\pm$  SE. First, normality of the distribution and equality of variance were tested with the Shapiro-Wilk normality and the Levene variance test. For data that were not normally distributed, the nonparametric Kruskal-Wallis test or Friedman test followed by Dunn's multiple comparisons test was used. For normally distributed data, a one-way ANOVA followed by a Tukey's multiple comparisons test was applied. Statistical analyses were conducted with GraphPad Prism 7 software, and calculations and graphs were made in Excel (Microsoft Office 2010) and Igor Pro (WaveMetrics).

### Immunohistochemistry

**Perfusion and tissue preparation.** Ten P33-P73 VGAT-ChR2-EYFP line eight mice (3 male, 7 female) were deeply anaesthetized by an intraperitoneal injection of a mixture of xylazine (2% Rompun and 7.95 mg/kg body wt Bayer) and ketamine (100 mg/ml Ketavet; Pfizer; 159 mg/kg body wt) in 0.9% NaCl. This was followed by transcardial perfusion with first 0.1 M phosphate buffer (pH 7.4) for 3 min and then with paraformaldehyde (Carl Roth; 4% in 0.1 M phosphate buffer, pH 7.4) for 15 min. The brains were immediately removed and postfixed overnight at  $4^\circ\text{C}$  in the 4% paraformaldehyde solution. The next day brains were thoroughly washed at room temperature with 0.1 M PBS, pH 7.4. Coronal sections ( $50 \mu\text{m}$ ) were cut at the level of the IC with a vibratome (VT1200; Leica Biosystems). The free-floating sections were rinsed three times in 0.1 M PBS (pH 7.4) for 10 min. To suppress nonspecific binding the sections were preincubated in 10% normal goat serum (NGS) or 10% normal donkey serum (NDS; GeneTex) with 0.2% Triton X-100 (Carl Roth) in PBS for 1 h at room temperature. Subsequently, the sections were incubated overnight at  $4^\circ\text{C}$  with either monoclonal mouse anti-HCN1 [1:1,000; University of California, Davis/National Institutes of Health NeuroMab Facility; cat. no.75-110; Research Resource Identifier (RRID):AB\_2115181]

rabbit anti-HCN2 (1:150; Alamone; RRID: AB\_2313726), and polyclonal goat anti-HCN4 (1:50; Santa Cruz Biotechnology; RRID: AB\_2248531), together with chicken anti-MAP2 (1:1,000; Neuromics; RRID: AB\_2314763) in 3% NGS or NDS with 0.2% Triton X-100 in PBS. All antibodies have previously been validated either by knockout experiments or Western blot (see manufacturer's home pages). Sections were then rinsed three times in PBS for 10 min and afterwards incubated for 2 h in the secondary antibody solution (3% NGS or NDS with 0.2% Triton X-100 in PBS) containing either Alexa 647 goat anti-mouse (1:200; Dianova), Cy5 goat anti-rabbit (1:300; Life Technologies), Alexa 633 donkey anti-goat (1:500; Invitrogen), or donkey anti-mouse DyLight 405 (1:400; Jackson ImmunoResearch), together with donkey anti-chicken Alexa 647 (1:500; Dianova). Negative controls were obtained by omitting the primary antibody. Afterwards, sections were rinsed again in PBS and two times in PB, mounted on slides, and coverslipped using a homemade antifading mounting media (Indig et al. 1997).

**Image acquisition.** Fluorescent micrographs were acquired using a confocal laser scanning microscope (TCS SP8; Leica Microsystems) equipped with a  $\times 5$  HCX PL FLUOTAR objective (NA 0.15),  $\times 20$  HC PL APO Imm Corr objective (0.75 NA), and a  $\times 63$  HC PL APO CS2 immersion-oil objective (1.4 NA). The pinhole was set to 1 Airy unit for each channel. Illumination and detection pathways were separated for each fluorophore, and individual color channels were sequentially acquired to avoid bleed-through artifacts. The acquisition settings were adjusted to cover the entire dynamic range of the detectors and remained unchanged during the course of the imaging process. The  $z$ -stacks of confocal images were obtained. Single optical sections or maximal projections of three single optical sections with thickness of  $0.27 \mu\text{m}$  were used for high-magnification figures. Images were further processed with ImageJ (Wayne Rasband, National Institutes of Health).

**Image analysis.** Image analysis was performed in Fiji (ImageJ Version 1.52i, National Institutes of Health). To quantify the relative HCN1 immunoreactivity across the dorso-ventral axis of the IC, we took image stacks at  $\times 5$  magnification in two to four sections from the middle of the rostral-caudal axis of the IC (5 ICs, 3 animals). Each stack consisted of four to six optical sections ( $z$ -distance:  $9$ – $11 \mu\text{m}$ ). Subsequently, average intensities were obtained over the entire  $z$ -stack for every pixel column. Mean gray values were calculated for  $50$ - $\mu\text{m}$  horizontal pixel columns at a distance of  $2.27 \mu\text{m}$  across the entire dorso-ventral axis of the IC. and normalized to the maximal value within each IC. The dorso-ventral extent of each IC was normalized from zero to one and divided into five regions. Normalized mean gray values were averaged for each of the five regions.

To quantify the number VGAT-EYFP+ neurons with HCN4+ perisomatic staining, stacks of five to six optical sections ( $z$ -distance:  $0.3 \mu\text{m}$ ) were obtained at  $\times 63$  magnification for three to five areas of interest distributed over the entire CIC (5 ICs, 3 animals). With the use of the Fiji Cell Counter, VGAT-EYFP+ neurons were visually identified and marked in each stack, carefully avoiding double counts. Each VGAT-EYFP+ neuron was subsequently scrutinized for HCN4 immunoreactivity around the somatic membrane and marked if a HCN4+ ring was present in more than one optical section. The total number of VGAT-EYFP+ with HCN4 ring and VGAT-EYFP+ without HCN4 ring was determined.

## RESULTS

We analyzed  $I_h$  properties for different populations and correlated them with firing behavior and passive membrane properties of GABAergic and non-GABAergic neurons in the central nucleus of the IC in young adult mice (postnatal days 22–28).  $I_h$  properties were also compared with the overall staining pattern of HCN1, HCN2, and HCN4 in the IC.

### Classification of GABAergic and Non-GABAergic Neurons in the IC

To discriminate between inhibitory (GABAergic) and excitatory (glutamatergic) neurons, we used the VGAT-ChR2-EYFP line 8 mouse (JAX stock no. 014548). In this model, ChR2 and EYFP are expressed under the control of the promoter of the VGAT, which enables optogenetic validation of VGAT+ neurons. Myelination at this age did not allow reliable optical verification of VGAT expression based on EYFP expression. We therefore classified neurons by their depolarization to light based on ChR2 expression. In about one third of the neurons blue light pulses (460–495 nm, 0.5–1 s) delivered through a  $\times 40$  objective induced a fast-activating and slowly inactivating inward current whereas the remaining two-thirds of the neurons did not show any current flow upon light stimulation (Fig. 1A). Since inhibitory and excitatory synaptic transmission were blocked during these experiments, the inward current was presumably induced by the opening of the Na<sup>+</sup>- and Ca<sup>2+</sup>-permeable ChR2 channels that are expressed in VGAT+ neurons. We therefore defined these neurons as GABAergic. In current-clamp mode, a blue light pulse induced a depolarization followed by bursts of action potentials in ~25% of the neurons that were VGAT+. In the remaining VGAT- neurons, light stimulation evoked a large transient hyperpolarization at the beginning of the stimulation and in many cases some small inhibitory postsynaptic potentials (IPSPs) later on (Fig. 1B). Both are likely to result from direct activation of presynaptic inhibitory terminals (Xie and Manis 2014) and to a lesser extent from somatic activation of connected GABAergic neurons. In some cases, neither an IPSP nor a depolarization with action potentials was observed during light stimulation. These neurons were also classified as VGAT-.

Immunostaining against GAD67 (Fig. 2, A–C, arrowheads), a marker for GABAergic neurons, in VGAT-EYFP channelrhodopsin mice showed that almost all neurons immunoposi-

tive for GAD67 also expressed EYFP in their membranes and to a lesser extent in the cytosol. In contrast, excitatory neurons lacked EYFP and GAD67 staining and were only MAP2+ (Fig. 2, B and D). This confirms previous results (Zhao et al. 2011) and shows that almost all neurons in the CIC expressing EYFP and channelrhodopsin are also GAD67+ and thus GABAergic. Since the IC is devoid of glycinergic neurons (Merchán et al. 2005) and all neurons either express the VGAT or the glutamate transporters VGluT1 or VGluT2 (Ito et al. 2011), we now refer to EYFP/VGAT- neurons as excitatory and EYFP/VGAT+ neurons as inhibitory neurons.

### I<sub>h</sub> Differs Between Excitatory and Inhibitory Neurons in the IC

I<sub>h</sub> was evoked in CIC neurons by voltage clamping the neurons to various holding potentials (from -55.5 mV to -120.5 mV; step size 5 mV), and I<sub>h</sub> properties were compared between inhibitory (VGAT+) and excitatory (VGAT-) neurons (Fig. 3). For all measurements, I<sub>h</sub> was pharmacologically isolated by bath application of blockers against several different voltage- and ligand-gated ion channels (see MATERIALS AND METHODS).

In all inhibitory neurons, hyperpolarizing voltage steps consistently triggered a slowly activating inward current (Fig. 3A<sub>1</sub>). In contrast, excitatory neurons displayed three different types of I<sub>h</sub>. First, neurons with a fast-activating and large I<sub>h</sub> amplitude (VGAT-, fast tau, Fig. 3A<sub>2</sub>); second, neurons with a slowly activating I<sub>h</sub> and a smaller I<sub>h</sub> amplitude (VGAT-, slow tau, Fig. 3A<sub>3</sub>); and third, neurons without I<sub>h</sub> (VGAT-, no I<sub>h</sub>, Fig. 3A<sub>4</sub>). The latter group of neurons did not display any slowly activating current during hyperpolarizing holding potentials.

Plotting I<sub>h</sub> amplitude against the activation time constant and half-maximal activation voltage indicated two groups of excitatory neurons with I<sub>h</sub> (Fig. 3B). One group displayed slowly activating I<sub>h</sub> (>235 ms, Fig. 3B, dashed line), hyperpolarized half-maximal activation voltage, and small I<sub>h</sub> amplitudes (VGAT-, slow tau), whereas the other group of neurons displayed large I<sub>h</sub> amplitude, faster activation time constants, and depolarized half-maximal activation voltages (VGAT-, fast tau). We chose an activation time constant of 235 ms to divide the population since, except for two intermediate neurons, neurons with >235-ms time constants consistently showed lower I<sub>h</sub> amplitudes and more hyperpolarized half-maximal voltage activation, similar to VGAT+ neurons. All inhibitory neurons (VGAT+) resembled the VGAT-, slow tau neurons, only with slightly larger I<sub>h</sub> amplitudes. Thirty-three percent of the neurons were VGAT+ and displayed slow-I<sub>h</sub> activation, 36% were VGAT- with fast-I<sub>h</sub> activation, and 25% were VGAT- with slow-I<sub>h</sub> activation. Only 6% did not exhibit any I<sub>h</sub> and were all VGAT- and thus excitatory (Fig. 3C).

I<sub>h</sub> densities, activation time constants, and half-maximal activation voltage were compared between the different groups of excitatory and inhibitory neurons. Current density was similar in VGAT+ and VGAT-, slow tau neurons but significantly larger in VGAT-, fast tau neurons when compared with the other groups (Table 1 and Fig. 3, D and D'). As expected, VGAT-, fast tau neurons displayed significantly faster I<sub>h</sub> activation time constants compared with VGAT+ and

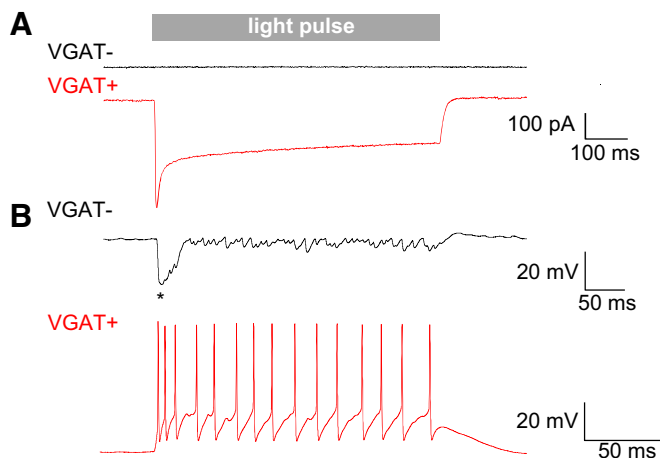


Fig. 1. Optogenetic validation of the GABAergic neurons expressing channelrhodopsin 2 (ChR2) vesicular GABA transporter-positive (VGAT+) and excitatory (VGAT-) neurons in the VGAT-ChR2-enhanced yellow fluorescent protein (EYFP) line 8 mouse in voltage (A) and in current clamp (B). In voltage-clamp experiments, TTX, DNQX, APV, and SR95531 were applied to the bath. Blue light pulses elicit an inward current (A) or action potentials (B) in VGAT+ neurons and a large inhibitory postsynaptic potential (IPSP) (\*) followed by small IPSPs in most VGAT- neurons (B).

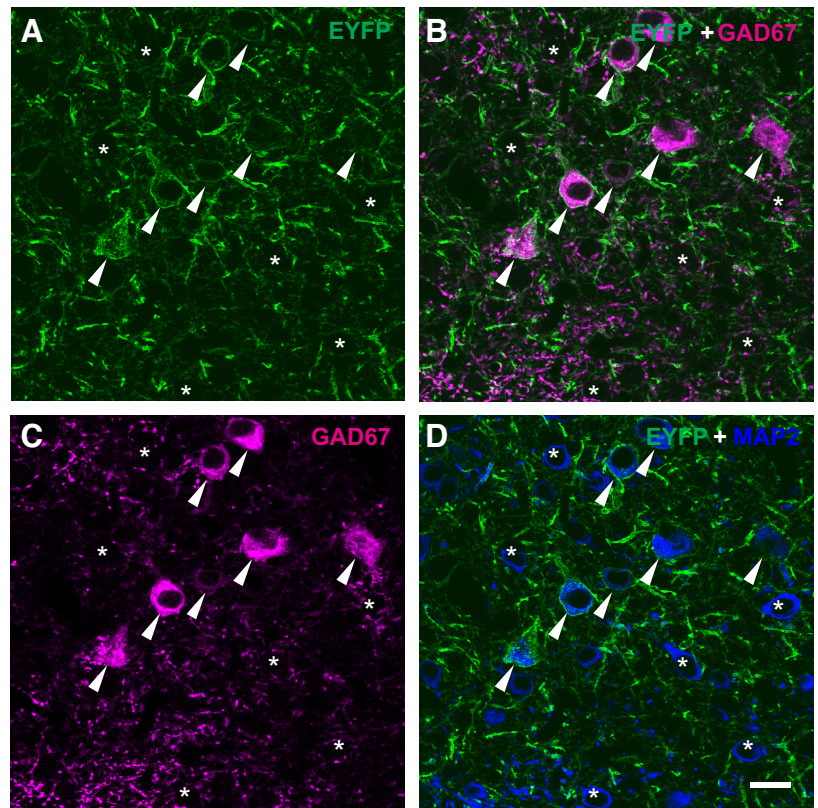


Fig. 2. Vesicular GABA transporter-positive (VGAT+) cells in the VGAT-channelrhodopsin 2 (ChR2)-enhanced yellow fluorescent protein (EYFP) line 8 mouse express EYFP (A, green, arrowheads). Staining for GAD67 (C and B, magenta) and MAP2 (D, blue) shows that EYFP+ cells colabel for GAD67 (B and D, arrowheads), whereas all EYFP- neurons are also GAD67- (\*). Scale bar = 20  $\mu$ m.

VGAT-, slow tau neurons (Table 1 and Fig. 3, E and E'). Similarly, the half-maximal activation voltage was significantly more negative in VGAT+ and VGAT-, slow tau neurons compared with VGAT-, fast tau neurons (Table 1, Fig. 3, F and F'). The differences in  $I_h$  kinetics and voltage dependence indicate that either HCN channel subtypes are differentially distributed in the various neuron types or that modulation of  $I_h$  via second messengers might be responsible for the observed differences.

#### GABAergic Neurons in the IC Are Positive for HCN4 and Lack HCN1 Immunoreactivity

To find out about the specific HCN channel types expressed in each group of neurons, we performed immunostaining procedures in paraformaldehyde-fixed IC sections against different HCN channel subtypes (HCN1, -2, and -4) and correlated them with the EYFP labeling in our VGAT-ChR2-EYFP mouse model. Labeling against HCN3 was omitted in this study, since HCN3 is mainly found in thalamic and olfactory neurons in the brain (Wahl-Schott and Biel 2009).

Profound HCN1 labeling was present around the somata of many neurons and in the neuropil in all parts of the CIC (Fig. 4, A<sub>1</sub> and D<sub>1</sub>). Interestingly, we observed many non-GABAergic, EYFP-negative neurons (Fig. 4A<sub>2</sub>, inset asterisks) with strong perisomatic labeling against HCN1 (Fig. 4A<sub>3</sub>, inset asterisks), whereas EYFP-positive GABAergic neurons did not show HCN1 immunoreactivity around their somata (Fig. 4A<sub>2</sub>, inset arrowheads; Fig. 4A<sub>3</sub>, inset arrowheads). This suggests that many excitatory, but no inhibitory, neurons express HCN1.

In contrast, HCN2-immunoreactivity was mainly somatic (Fig. 4B<sub>1</sub>, inset asterisks and arrowheads) and abundantly

expressed in CIC neurons, irrespective whether they were EYFP positive (Fig. 4, B<sub>2</sub> and B<sub>3</sub>, inset arrowheads) or EYFP negative (Fig. 4, B<sub>2</sub> and B<sub>3</sub>, inset asterisks).

HCN4 immunoreactivity was mostly perisomatic (Fig. 4C<sub>1</sub>, inset arrowheads and asterisk) and was present in almost all EYFP-positive, GABAergic neurons (Fig. 4, C<sub>2</sub> and C<sub>3</sub>, inset arrowheads). Ninety-six percent of EYFP-positive neurons showed HCN4+ rings (74 neurons out of 77 neurons). Perisomatic HCN4 labeling was also observed in a number of non-GABAergic neurons (Fig. 4, C<sub>2</sub> and C<sub>3</sub>, inset asterisks).

We conclude from these experiments that GABAergic neurons in the IC exhibit  $I_h$  that is mainly transmitted via ion channels composed of HCN2 and HCN4 subunits. In contrast, different types of excitatory neurons exist, with either fast  $I_h$  transmitted via HCN1/HCN2, or slow  $I_h$  transmitted via HCN2 and in some cases HCN4.

As HCN1 has been shown to be tonotopically organized in the rat IC (Koch et al. 2004) we quantified whether a similar differential distribution of HCN1 was also present in the mouse IC (Fig. 4D). We measured mean gray values of HCN1 immunostaining for a 50- $\mu$ m wide rectangle spanning along the dorso-ventral axis of the IC (Fig. 4D<sub>1</sub>). Quantification of HCN1 mean gray value along the dorso-ventral extent of the IC ( $n = 5$ ) revealed no systematic gradient of HCN1 immunoreactivity within the CIC (Fig. 4D<sub>3</sub>) ( $P = 0.66$ ; Friedman test with Dunn's multiple comparison). In the ICs, the most dorsal 20% part was located in the ECIC, where HCN1 immunoreactivity was profoundly lower as previously shown (Koch et al. 2004). This suggests that in the mouse IC, HCN1+ neurons with large and fast  $I_h$ , are unlikely to be more present in the ventral part compared with the dorsal part of the CIC.

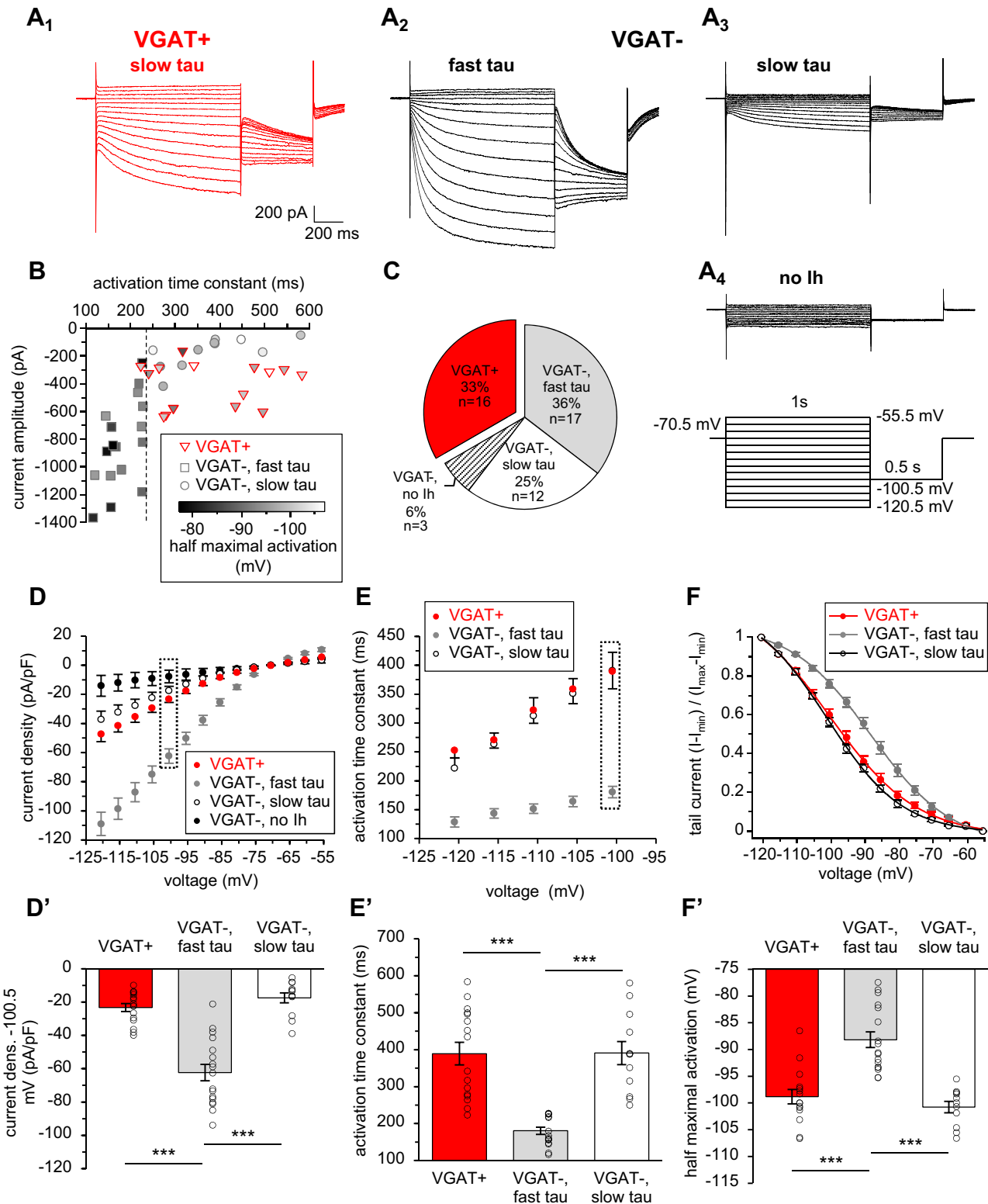


Fig. 3. Representative examples of isolated hyperpolarizing-activated current ( $I_h$ ) in GABAergic vesicular GABA transporter-positive (VGAT+) ( $A_1$ ) and different non-GABAergic (VGAT-) neurons ( $A_2$ - $A_4$ ) classified according to  $I_h$  activation time constant ( $\tau$ ) into slow ( $A_1$  and  $A_3$ ), fast ( $A_2$ ), and neurons without  $I_h$  ( $A_4$ ). Relationship between activation time constant, half-maximal activation, and current amplitude ( $B$ ) in GABAergic and non-GABAergic neurons. The dotted line separates non-GABAergic cells into fast- and slow tau neurons. Distribution of the 4  $I_h$  kinetic cell types ( $C$ ). Quantification of  $I_h$  properties of GABAergic and different non-GABAergic neurons ( $D$ - $F'$ ). GABAergic neurons have significantly smaller current density ( $D$  and  $D'$ ), slower  $I_h$  ( $E$  and  $E'$ ), and lower half maximal activation ( $F$  and  $F'$ ) compared with the population of non-GABAergic neurons with fast  $I_h$ . Dashed boxes in  $D$  and  $E$  are values represented in  $D'$  and  $E'$ . Kruskal-Wallis test followed by Dunn's multiple comparisons test (\*\*\*)  $P < 0.001$ .

Table 1. Comparison of pharmacologically isolated  $I_h$ -current parameters in VGAT+ and different groups of VGAT- neurons

	$I_h$ Activation Time Constant, ms	Dunn's Multiple Comparisons Test	Current Density, pA/pF	Dunn's Multiple Comparisons Test	Half Maximal Activation, mV	Dunn's Multiple Comparisons Test
VGAT+	389 ± 30 (16)	VGAT-, fast tau***	-23.2 ± 2.4 (16)	VGAT-, fast tau***	-98.8 ± 1.3 (15)	VGAT-, fast tau***
VGAT-, fast tau	181 ± 10 (17)	VGAT-, slow tau***	-62.3 ± 4.9 (17)	VGAT-, slow tau***	-88.2 ± 1.5 (17)	VGAT-, slow tau***
VGAT-, slow tau	391 ± 31 (12)		-17.4 ± 3.0 (12)		-100.8 ± 1.1 (11)	

All the parameters are given in means ± SE (number of neurons). Vesicular GABA transporter-negative (VGAT-) neurons with fast-activating  $I_h$  were significantly different from the group of VGAT+ neurons and VGAT-, slow tau neurons for all  $I_h$  parameters. Statistical significance of difference between VGAT+, VGAT- with fast  $I_h$  tau, and VGAT- and slow  $I_h$  tau neurons was calculated using Kruskal-Wallis test followed by Dunn's multiple comparisons test \*\*\* $P < 0.001$ .

### GABAergic Neurons Are All Adapting Firing Whereas non-GABAergic Neurons Display a Range of Different Firing Patterns

We next wanted to find out whether  $I_h$  properties and HCN subtype distribution were correlated with the different firing patterns observed in GABAergic and non-GABAergic IC neurons. We recorded voltage responses to 0.5-s hyperpolarizing and depolarizing current pulses and analyzed  $I_h$  activation, passive membrane properties and firing behavior in VGAT+ and VGAT- neurons. Almost all GABAergic neurons showed an adapting firing pattern (Fig. 5A<sub>1</sub>), while non-GABAergic neurons exhibited both onset (Fig. 5A<sub>2</sub>) and adapting firing patterns (Fig. 5A<sub>3-5</sub>) with different  $I_h$ -sag characteristics (Fig. 5, A and B). To obtain a quantitative correlate of  $I_h$  activation kinetics, the depolarization slope during -200-pA hyperpolarization current injections was fit with an exponential function. Additionally, relative  $I_h$ -sag amplitude (see MATERIALS AND METHODS) was calculated to obtain a correlate of  $I_h$  amplitude in each neuron. We are aware that these two parameters only partially correlate with  $I_h$  amplitude and  $I_h$  activation time constant but also depend on membrane capacitance and the activation of other voltage-gated ion channels in the respective neurons. Using these two parameters as a criterion, we were able to group VGAT+ and VGAT- neurons comparable to the groups formed upon differences in  $I_h$  properties (Fig. 5B). VGAT+ neurons displayed  $I_h$  sags with relatively slow kinetics (>70 ms) and small amplitudes (<50%) (Fig. 5, A<sub>1</sub>, C, and D). VGAT- neurons displayed different  $I_h$ -sag characteristics. All VGAT- onset firing neurons had fast  $I_h$ -sag activation (<70 ms) and large  $I_h$ -sag amplitudes (>50%), whereas VGAT- adapting neurons could be divided into three groups according to their  $I_h$ -sag properties (Fig. 5, A<sub>2-5</sub>, C, and D, and Table 2). About half of the VGAT- neurons displayed fast-activating (<70 ms) and large  $I_h$ -sag amplitudes, similar to the onset firing neurons, whereas the other half of VGAT- neurons displayed slow-activating and low-amplitude  $I_h$  sags, more resembling the VGAT+ neurons (Fig. 5, C and D). Again, a few neurons showed no apparent  $I_h$  activation. Gen-

erally, the relative number of neurons in each group was similar to the relative group sizes based on  $I_h$  measurements (Figs. 3C and 5B).

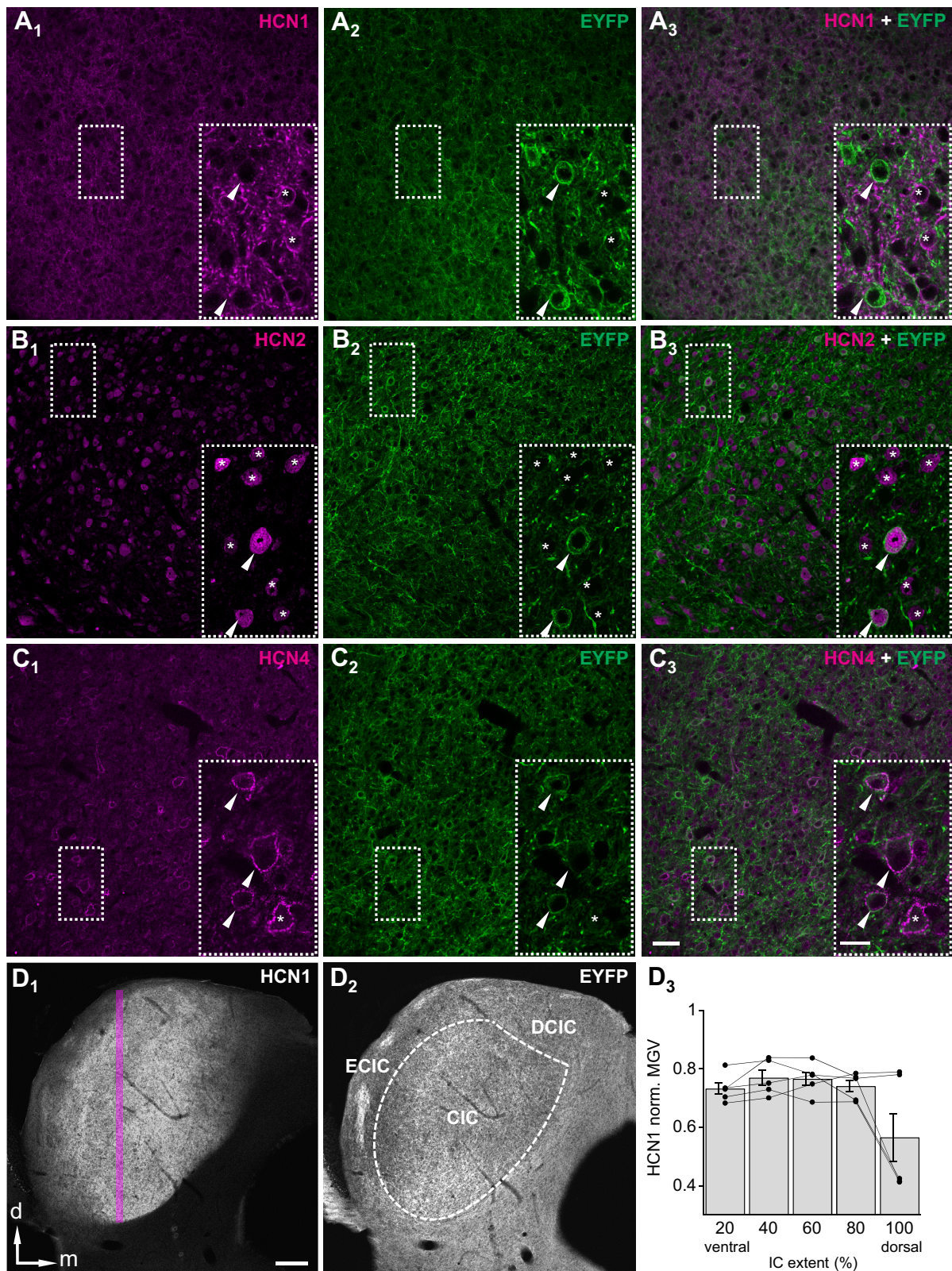
We next compared passive membrane parameters, such as resting membrane potential, input resistance, and membrane time constant, between VGAT+ and the different groups of VGAT- neurons. All these parameters were significantly different between VGAT+ neurons and VGAT- onset firing neurons (Fig. 5, E-G and Table 3). Also, VGAT- groups differed from each other for many of these parameters. To conclude, VGAT+ neurons are not significantly different from many VGAT- neuron types in terms of membrane properties and  $I_h$ , whereas the VGAT- onset type neurons seem to be a separate class of neurons.

As shown in the examples in Fig. 5, A<sub>2</sub> and A<sub>3</sub>, some neurons displayed rebound firing after prolonged hyperpolarization. We determined the relative number of neurons that displayed rebound spiking in response to a hyperpolarization reaching -91.5 mV at steady state (Fig. 3H), a value that is close to the Cl<sup>-</sup> reversal potential in those neurons (Vale and Sanes 2002). A hyperpolarization to -90.5 mV triggered a rebound spike in all VGAT- onset firing neurons. Also, 80% of the VGAT- adapting firing neurons with fast  $I_h$  exhibited rebound spiking, whereas only few VGAT+ or VGAT- slow- $I_h$  neurons showed rebound responses. This indicates that rebound firing is facilitated by large and fast-activating  $I_h$  and mainly found in specific subclasses of IC neurons.

### Adapting Firing GABAergic and Non-GABAergic Neurons Display Small Differences in Their Spike Rate Adaptation

The large majority (88%) of neurons in the IC adapted their firing to depolarizing current injections, regardless of neurotransmitter phenotype. However, adapting firing patterns can vary in their maximal firing rate, in their rate-level relationship, and in their firing adaptation pattern. We therefore analyzed these parameters for all adapting firing neurons and compared them between VGAT+ and the different groups of VGAT-

Fig. 4. Hyperpolarization-activated and cyclic-nucleotide-gated (HCN1; A), HCN2 (B), and HCN4 (C) immunoreactivity (magenta) in the central nucleus of inferior colliculus (CIC) of the transgenic VGAT-ChR2-EYFP line 8 mouse, GABAergic (VGAT+) neurons express EYFP (green, arrowheads), and non-GABAergic neurons lack of EYFP immunoreactivity (\*). HCN1 is absent in GABAergic neurons but present in many non-GABAergic neurons (A). HCN2-immunoreactivity is present in GABAergic as well non-GABAergic neurons (B). HCN4-immunoreactivity is present in GABAergic as well as in some non-GABAergic neurons (C). Scale bar = 50 μm, inset = 20 μm. Representative overview (×5) of HCN1 (D<sub>1</sub>) and EYFP (D<sub>2</sub>) immunoreactivity in the entire inferior colliculus (scale bar = 250 μm). The rectangle represents the area where mean gray values (MGVs) of HCN1 immunostainings were measured (D<sub>1</sub>). EYFP fluorescence with the boundaries of the central nucleus (CIC), the external cortex (ECIC), and the dorsal cortex (DCIC) of the inferior colliculus (D<sub>2</sub>). Quantification of MGV of HCN1 immunostaining along the dorso-ventral extent of the inferior colliculus (D<sub>3</sub>). No gradient of HCN1 staining was observed along the dorso-ventral (tonotopic) axis within the CIC. Friedman test followed by Dunn's multiple comparisons test. EYFP, enhanced yellow fluorescent protein; VGAT, vesicular GABA transporter.



neurons. Figure 6A<sub>1-4</sub> shows representative voltage responses and dot displays of spikes for each group.

We first analyzed spike rates for depolarizing current pulses and plotted them against the amplitude of injected current

above the firing threshold. Averaging of these firing rate-level relationships did not yield any difference between VGAT+ and VGAT- groups (Fig. 6B). Also, average firing rates (at 200 pA above firing threshold) did not statistically differ

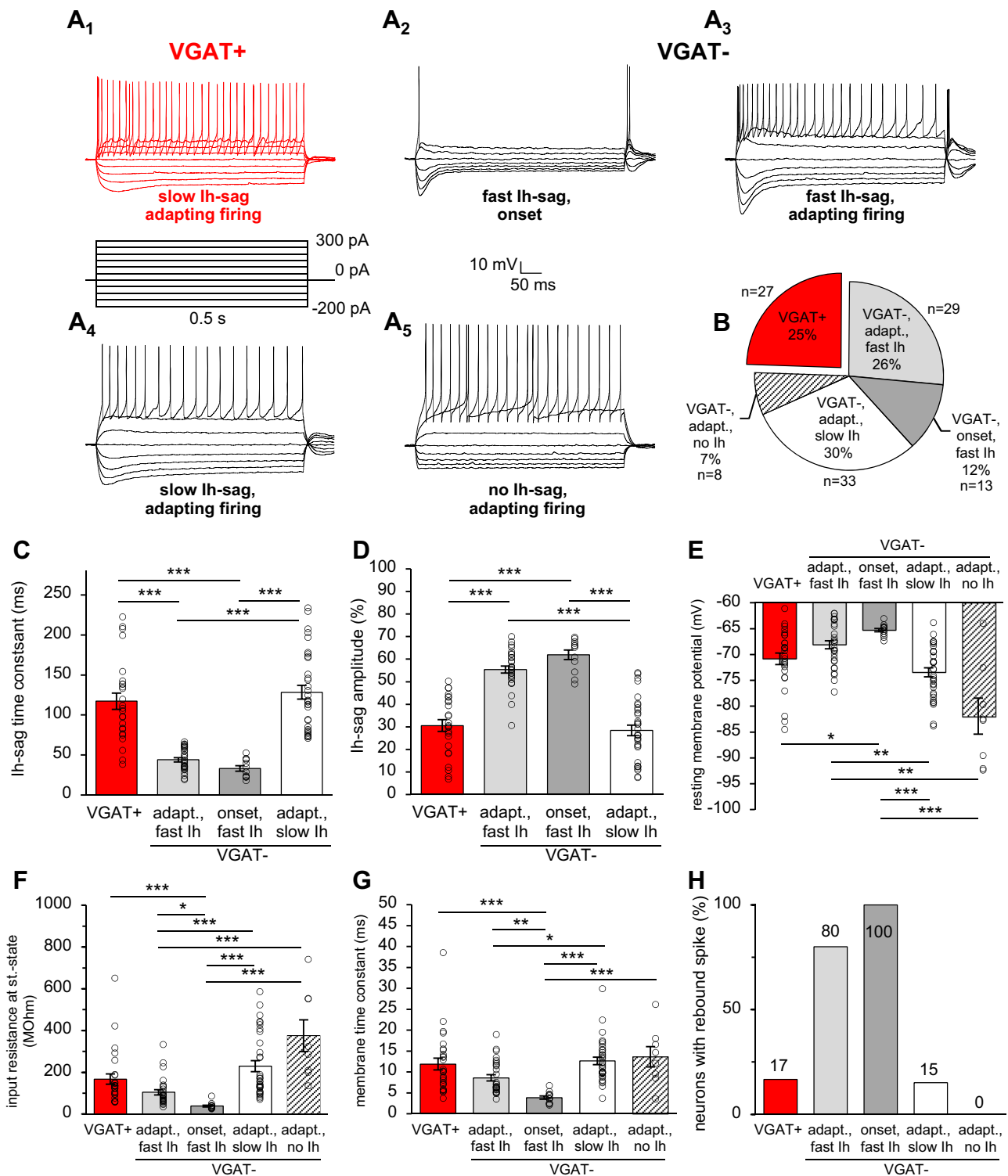


Fig. 5. Representative voltage responses to step current injections for different vesicular GABA transporter-positive (VGAT+) and VGAT- cell types ( $A_1$ – $A_5$ ). All GABAergic neurons (VGAT+) display adapting firing pattern and slowly depolarizing voltage sag ( $A_1$ ). Non-GABAergic neurons (VGAT-) show variable firing patterns: onset ( $A_2$ ) or adapting firing with different kinetic of the depolarizing voltage sag ( $I_h$ -sag): fast ( $A_3$ ), slow ( $A_4$ ), or absence of  $I_h$ -sag ( $A_5$ ). Distribution of  $I_h$ -sag kinetic types ( $B$ ).  $I_h$ -sag time constant is significantly larger in VGAT+ than in VGAT- onset and VGAT- adapting firing neurons with fast  $I_h$  ( $C$ ).  $I_h$ -sag amplitude ratio is significantly smaller in VGAT+ neurons than in VGAT- onset and adapting firing neurons with fast- $I_h$  sag ( $D$ ). Resting membrane potential ( $E$ ), input resistance of steady state ( $F$ ), and membrane time constant ( $G$ ) are significantly different between VGAT+ and VGAT- onset neurons. Most VGAT- neurons with fast  $I_h$  show rebound spikes, whereas only few neurons with slow  $I_h$  (VGAT+ or VGAT-) display rebound spiking ( $H$ ) Kruskal-Wallis test followed by Dunn's multiple comparisons test ( $*P < 0.05$ ,  $**P < 0.01$ ,  $***P < 0.001$ ).

Table 2. Comparison of I<sub>h</sub>-sag properties of VGAT+ and different groups of VGAT- neurons

	I <sub>h</sub> Sag, %	Dunn's Multiple Comparisons Test	I <sub>h</sub> Time Constant, ms	Dunn's Multiple Comparisons Test	n
VGAT+	30.6 ± 2.6	VGAT-, fast I <sub>h</sub> *** VGAT-, onset***	117.2 ± 10.3	VGAT-, fast I <sub>h</sub> *** VGAT-, onset***	25
VGAT-, adapt., fast I <sub>h</sub>	55.4 ± 1.5	VGAT-, slow I <sub>h</sub> ***	44.1 ± 2.6	VGAT-, slow I <sub>h</sub> ***	29
VGAT-, onset, fast I <sub>h</sub>	62.0 ± 2.1	VGAT-, slow I <sub>h</sub> ***	33.2 ± 3.4	VGAT-, slow I <sub>h</sub> ***	12
VGAT-, adapt., slow I <sub>h</sub>	28.5 ± 2.3		128.6 ± 8.6		33

All the parameters are given in means ± SE. Statistical significance of difference between vesicular GABA transporter-positive (VGAT+), VGAT- onset, adapting firing VGAT- neurons with fast I<sub>h</sub>, and adapting firing VGAT- neurons with slow I<sub>h</sub> was calculated using Kruskal-Wallis test followed by Dunn's multiple comparisons test \*\*\*P < 0.001.

between VGAT+ and the various VGAT- groups (Fig. 6C) [in Hz: VGAT+: 115 ± 10 (n = 25); VGAT- (fast I<sub>h</sub>): 117 ± 11 (n = 19); VGAT- (slow I<sub>h</sub>): 117 ± 7 (n = 18); VGAT- (no I<sub>h</sub>): 109 ± 13 (n = 5); P = 0.98; one-way ANOVA with Tukey's test].

To compare adaptation rate between different VGAT+ and VGAT- groups, we plotted average firing frequencies (calculated from interspike intervals) for each group (Fig. 6, A and D). On average, VGAT+ neurons displayed a rapid spike rate adaptation during the first 200 ms but did not adapt much thereafter (Fig. 6D). In contrast, all VGAT- cell types showed a more prolonged spike adaptation throughout the entire stimulus (Fig. 6D). We quantified adaptation for each neuron by fitting a double-exponential curve to the successive spike frequency plot obtained by calculating the firing frequency between the first spike and every following spike and plotting them against the time points of the respective following spike (see MATERIALS AND METHODS). Adaptation rates, expressed as weighted tau, were significantly faster (smaller weighted tau) in VGAT+ neurons compared with VGAT- slow and VGAT- no I<sub>h</sub> neurons (Fig. 6E), whereas as adaptation did not significantly differ between other neuron types [in ms: VGAT+: 69 ± 11 (n = 24); VGAT- (fast I<sub>h</sub>): 153 ± 58 (n = 24); VGAT- (slow I<sub>h</sub>): 167 ± 32 (n = 30); VGAT- (no I<sub>h</sub>): 541 ± 280 (n = 7), Kruskal-Wallis test followed by Dunn's multiple comparisons test (P < 0.01)].

## DISCUSSION

The present study compares I<sub>h</sub> properties, HCN channel subtype distribution, and firing pattern between GABAergic and non-GABAergic neurons in the central nucleus of the IC in young adult mice. All GABAergic neurons displayed slowly activating I<sub>h</sub> and expressed mainly HCN2 and HCN4 subunits

and an adapting firing pattern to depolarizing currents. In contrast, I<sub>h</sub> properties and firing patterns were more diverse in glutamatergic neurons. About 15% of the glutamatergic neurons displayed onset firing with fast-activating I<sub>h</sub>. The remaining glutamatergic neurons had an adapting firing pattern and displayed slow- or fast-activating I<sub>h</sub>.

By using a transgenic mouse line that expresses EYFP and channelrhodopsin under the promotor of the VGAT, we were able to unambiguously identify the presence or absence of VGAT by blue light stimulation, in young adult brain slices (Caspari et al. 2015; Zhao et al. 2011). Since channelrhodopsin also inserts in GABAergic presynaptic terminals, light produced strong hyperpolarization in both excitatory and inhibitory neurons as described previously (Ono et al. 2016). First, it is unlikely that a constitutive activation of channelrhodopsin channels altered the response properties of GABAergic neurons since previous studies that investigated intrinsic firing properties of IC neurons in a different mouse model came up with similar populations according to firing patterns (Ono et al. 2005; Tan et al. 2007). Second, a previous study, using the same VGAT-EYFP-channelrhodopsin mouse model, showed that spike patterns of IC neurons in response to sounds were not noticeably altered compared with wild-type mice (Ono et al. 2017). Third, both resting membrane potential and input resistance were comparable between excitatory and inhibitory neurons in our study, which argues against a constitutive activation of depolarizing ion channels.

### Differential distribution of HCN Channel Subtypes and I<sub>h</sub> Properties in Excitatory and Inhibitory IC Neurons

One interesting result of our study was a lack of HCN1 staining around VGAT-EYFP+ and thus GABAergic cell somata. This suggests that HCN1 channels are exclusively

Table 3. Comparison of passive membrane properties of VGAT+ and different groups of VGAT- neurons

	Resting Potential, mV	Dunn's Multiple Comparisons Test	Input Resistance at Steady State, MΩ	Dunn's Multiple Comparisons Test	Membrane Time Constant, ms	Dunn's Multiple Comparisons Test	n
VGAT+	-70.8 ± 1.1	VGAT-, onset*	167.7 ± 24.7	VGAT-, onset***	11.9 ± 1.4	VGAT-, onset***	27
VGAT-, adapt., fast I <sub>h</sub>	-68.1 ± 0.8	VGAT-, slow I <sub>h</sub> ** VGAT-, no I <sub>h</sub> **	104.2 ± 12.2	VGAT-, onset* VGAT-, slow I <sub>h</sub> *** VGAT-, no I <sub>h</sub> ***	8.6 ± 0.7	VGAT-, onset** VGAT-, slow I <sub>h</sub> *	29
VGAT-, onset, fast I <sub>h</sub>	-65.3 ± 0.3	VGAT-, slow I <sub>h</sub> *** VGAT-, no I <sub>h</sub> ***	38.4 ± 4.4	VGAT-, slow I <sub>h</sub> *** VGAT-, no I <sub>h</sub> ***	3.9 ± 0.4	VGAT-, slow I <sub>h</sub> *** VGAT-, no I <sub>h</sub> ***	13
VGAT-, adapt., slow I <sub>h</sub>	-73.4 ± 0.9		229.6 ± 26.1		12.6 ± 0.9		33
VGAT-, adapt., no I <sub>h</sub>	-81.9 ± 3.5		375.2 ± 76.1		13.6 ± 2.4		8

All parameters are given in means ± SE. Statistical significance of difference between vesicular GABA transporter-positive (VGAT+), VGAT- onset, adapting firing VGAT- neurons with fast I<sub>h</sub>, and adapting firing VGAT- neurons with slow I<sub>h</sub> or absent I<sub>h</sub> was calculated using Kruskal-Wallis test followed by Dunn's multiple comparisons test \*P < 0.05, \*\*P < 0.01, \*\*\*P < 0.001.

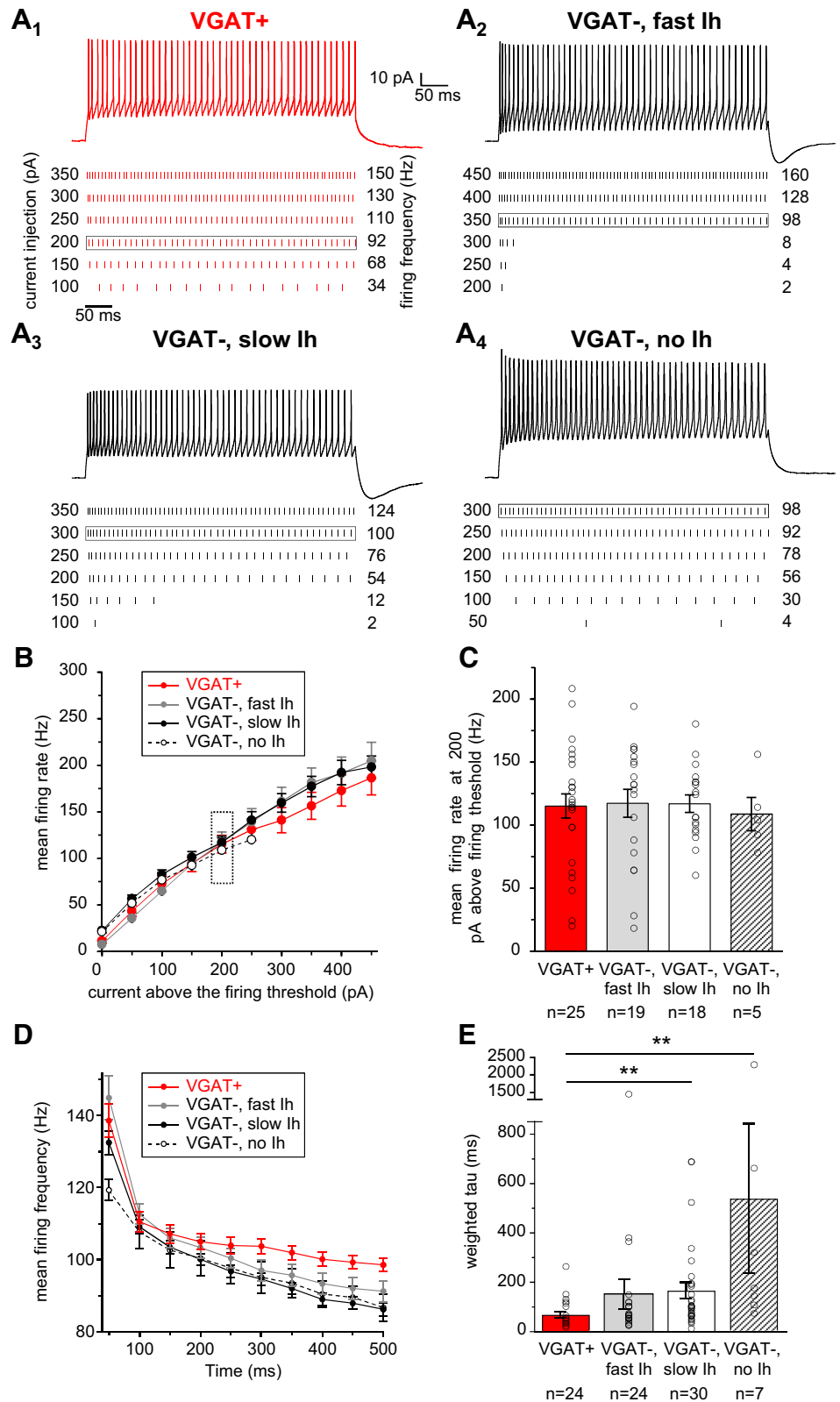


Fig. 6. Firing and adapting properties of the vesicular GABA transporter-positive (VGAT+) and adapting firing VGAT- neurons. Exemplary raster plots and membrane-voltage responses with firing rates close to 100 Hz (average  $102 \pm 11$  Hz) (box depicts corresponding raster plot) for analysis of adapting properties of VGAT+ ( $A_1$ ) and VGAT- with fast  $I_h$  ( $A_2$ ) and VGAT-, slow  $I_h$  ( $A_3$ ), and VGAT- without  $I_h$  neurons ( $A_4$ ). Averaged firing rates ( $B$ ) versus injected current amplitude for different VGAT+ and VGAT- neurons. Mean firing rates for injected currents 200 pA above the firing threshold ( $C$ , dotted case in  $B$ ); there were no significant differences between the four groups on neurons detected (one-way ANOVA with Tukey's multiple comparisons test). Average spike frequency histograms (bin width: 50 ms) of VGAT+ ( $n = 24$ ); VGAT-, fast  $I_h$  ( $n = 24$ ); VGAT-, slow  $I_h$  ( $n = 30$ ); and VGAT-, no  $I_h$  ( $n = 7$ ) neurons ( $D$ ). Adaptation rates ( $E$ ) calculated as weighted taus for successive spike frequency plots show that VGAT+ neurons adapt significantly faster compared with the VGAT- slow  $I_h$  and VGAT- no  $I_h$  neurons. Kruskal-Wallis test followed by Dunn's multiple comparisons test (\*\* $P < 0.01$ ). Data are shown as means  $\pm$  SE.

expressed in excitatory, HCN4 mainly in inhibitory neurons whereas HCN2 is abundantly expressed in excitatory and inhibitory neurons. This was corroborated by the physiological  $I_h$  properties measured in the different cell types. Previous studies have identified fast and slow  $I_h$  in different subpopu-

lations of the IC (Koch and Grothe 2003; Nagtegaal and Borst 2010); however, this had not been related to different neurotransmitter types. One intriguing question is, what is the functional role of the differences in  $I_h$  in excitatory and inhibitory neurons?

Generally,  $I_h$  activation has complex and sometimes opposing effects on the integration of excitatory and inhibitory inputs and the firing of neurons (Shah 2018).  $I_h$  activation depolarizes the membrane potential thus increasing the probability of inputs to reach spike threshold. However, this is also dependent on whether the firing threshold is positive or negative to the reversal potential of  $I_h$ , which has been measured to be between  $-35$  and  $40$  mV (Bal and Oertel 2000; Funahashi et al. 2003). On the contrary,  $I_h$  decreases the input resistance thereby decreasing the effectiveness of each incoming input to reach spike threshold. Moreover, depolarization of the resting membrane potential by  $I_h$  keeps neurons closer to the firing threshold despite profound inhibitory inputs (Baumann et al. 2013). Another major effect of  $I_h$  together with its counterplayer the low-voltage-activated potassium channels is a lowering the temporal summation of both excitatory and inhibitory synaptic inputs (Khurana et al. 2011; Koch and Grothe 2003; Nagtegaal and Borst 2010). Thus neurons with large and fast-activating  $I_h$  typically show less temporal integration of synaptic inputs and are best suited to faithfully transmit the temporal pattern of sound information (Khurana et al. 2012; Oertel 1999). In contrast, slowly activating  $I_h$  or absence of  $I_h$  facilitates temporal integration of acoustic inputs (Nagtegaal and Borst 2010).  $I_h$  transmitted by channels composed of the different subunits HCN1–4 also differs in gating, voltage dependence and the potential to be modulated by second messengers. HCN4 channels are, as opposed to HCN1 channels, strongly modulated by second messengers like cAMP or other molecules like anions or tyrosine kinases (Viscomi et al. 2001; Wahl-Schott and Biel 2009). By accelerating the activation time constants of  $I_h$  and depolarizing the half-maximal activation, these modulators may change the integrative properties of these neurons (Khurana et al. 2012). Since HCN4 channels are primarily expressed in GABAergic neurons, neuromodulatory inputs that increase intracellular second messenger concentration (e.g., serotonin) may predominantly target the integrative properties of the GABAergic population (Hurley et al. 2008; Ko et al. 2016).

#### *GABAergic Neurons Share similar $I_h$ Properties and Firing Pattern*

In our study, all GABAergic neurons showed a slowly activating  $I_h$ , expressed HCN4 channels, and had an adapting firing pattern with various degrees of adaptation. Based on these measurements, the population of GABAergic neurons could not be further divided. However, it is possible that more physiological subclasses of GABAergic neurons exist since brain slice preparation and recording configurations may have biased our sample toward one neuron type. Moreover, other GABAergic neuron types with low prevalence (10% or lower) may have escaped our sample due to our relatively low sample size. It is also possible that further physiological measurements or molecular profiling may reveal different populations of GABAergic IC neurons. This shows the need for a more detailed analysis including molecular profiling, and additional analyses of input/output connectivity to reach a better understanding of GABAergic neuron types in the IC, similar to previous attempts in the neocortical structures (Tremblay et al. 2016).

Several recent studies have identified two main types of GABAergic neurons in the IC according to the firing pattern or input-output connections (Beebe et al. 2016; Ito et al. 2009; Ono et al. 2005). In one study, in which GABAergic neurons in the IC were visually identified upon their GAD67-GFP labeling, a large proportion of GABAergic neurons in the CIC were regular spiking with some degree of adaptation (Ono et al. 2005). The same study also identified a population of GABAergic neurons with build-up or/and pause response, a firing pattern that we did not observe in the CIC. One possible explanation for this is a reduction in build-up and pause patterns as neurons mature. In fact, only few neurons in the study from Ono et al. (2005) were from animals older than postnatal *day 13*. This is corroborated by the fact that adult mice show only weak expression of Kv4.2 and Kv4.3, the channels underlying the A-current and the build-up and pause response pattern (Grimsley et al. 2011; Oliver 2000). Also, input resistance and time constants were considerably lower in the present study compared with the previous study (Ono et al. 2005) indicating that membrane properties in the IC mature beyond the age of postnatal *day 18*. Other studies have grouped GABAergic CIC neurons according to anatomical criteria. About 60% of GABAergic neurons, which also have larger soma diameters, receive a prominent ring of VGluT2+ excitatory inputs on the soma, whereas the remaining GABAergic neurons, with smaller soma diameters, do not show this VGluT2+ ring (Beebe et al. 2016; Ito et al. 2009, 2016). The most likely sources of these inputs are the dorsal cochlear nucleus, the medial and lateral superior olive, the intermediate ventral nucleus of the lateral lemniscus, and the IC neurons themselves (Ito and Oliver 2010). These large GABAergic neurons with VGluT2 somatic inputs provide a rapid inhibitory input to the medial geniculate body (Geis and Borst 2013; Ito et al. 2009). Although we have seen a similar distribution of somatic VGluT2-input+ and VGluT2-input- GABAergic neurons in the mouse IC (data not shown), we were not able to separate two distinct groups of GABAergic neurons according to  $I_h$  measurements. This was also seen in a recent *in vivo* study where two distinct groups of GABAergic CIC neurons according to their firing pattern in response to acoustic stimulation were indistinguishable (Ono et al. 2017). This is different from many GABAergic interneurons in the cortex and hippocampus, which can be readily distinguished from excitatory neurons based on their active and passive membrane properties and firing pattern.

#### *A Small Set of Excitatory Neurons Resemble Neurons in the Medial and Lateral Superior Olive*

All neurons that fired one or a few action potentials only at the beginning of the depolarization were non-GABAergic and thus excitatory. These neurons had low input resistance and displayed fast-activating, large-amplitude  $I_h$  most likely mediated by HCN1 channels. These membrane properties resemble the membrane properties of principal neurons in the lateral and medial superior olive, which express high levels of HCN1 and low voltage-activated potassium (Kv1.x) channels (Barnes-Davies et al. 2004; Hassfurth et al. 2009; Khurana et al. 2011, 2012; Leao et al. 2006). In these neurons, the properties of HCN1 channels and low-voltage-activated K+ channels ( $K_{LT}$ ), create low input re-

sistance around the resting membrane potential, which enables them to integrate excitatory and inhibitory inputs on an extremely rapid and precise time scale (Magnusson et al. 2005; Scott et al. 2005; Walcher et al. 2011). Kv1.1 channels are also expressed in a subset of IC neurons (Rosenberger et al. 2003) with a tonotopic distribution similar to HCN1 channels in some species (Koch et al. 2004). It is thus likely that the population of excitatory IC neurons with this set of ion channels show similar properties to neurons in the superior olive with high phase-locking ability to the envelope of temporally structured sounds (Ashida et al. 2016). This population of excitatory IC neurons may also correspond to the small percentage of excitatory neurons in the IC that show high-pass modulation transfer functions in response to temporally structured sounds (Ono et al. 2017). Future studies dissecting the anatomical inputs and outputs of this specific population of excitatory neurons and targeted recordings of their spike response to acoustic stimulation will help to elucidate their role in auditory processing.

#### ACKNOWLEDGMENTS

We thank Karin Heufelder for installing the breeding colony and technical assistance. We also thank Anna Magnusson for comments on an earlier version of this manuscript.

#### GRANTS

This work was supported by the Deutsche Forschungsgemeinschaft SFB665 to U. Koch.

#### DISCLOSURES

No conflicts of interest, financial or otherwise, are declared by the authors.

#### AUTHOR CONTRIBUTIONS

V.N., J.H., and U.K. conceived and designed research; V.N. and J.H. performed experiments; V.N., J.H., F.d.A., and U.K. analyzed data; V.N., J.H., and U.K. interpreted results of experiments; V.N., J.H., F.d.A., and U.K. prepared figures; V.N., J.H., and U.K. drafted manuscript; V.N., J.H., F.d.A., and U.K. edited and revised manuscript; V.N., J.H., F.d.A., and U.K. approved final version of manuscript.

#### REFERENCES

- Ashida G, Kretzberg J, Tollin DJ. Roles for coincidence detection in coding amplitude-modulated sounds. *PLoS Comput Biol* 12: e1004997, 2016. doi:10.1371/journal.pcbi.1004997.
- Bal R, Oertel D. Hyperpolarization-activated, mixed-cation current (I<sub>h</sub>) in octopus cells of the mammalian cochlear nucleus. *J Neurophysiol* 84: 806–817, 2000. doi:10.1152/jn.2000.84.2.806.
- Barnes-Davies M, Barker MC, Osmani F, Forsythe ID. Kv1 currents mediate a gradient of principal neuron excitability across the tonotopic axis in the rat lateral superior olive. *Eur J Neurosci* 19: 325–333, 2004. doi:10.1111/j.0953-816X.2003.03133.x.
- Baumann VJ, Lehnert S, Leibold C, Koch U. Tonotopic organization of the hyperpolarization-activated current (I<sub>h</sub>) in the mammalian medial superior olive. *Front Neural Circuits* 7: 117, 2013. doi:10.3389/fncir.2013.00117.
- Beebe NL, Young JW, Mellott JG, Schofield BR. Extracellular Molecular Markers and Soma Size of Inhibitory Neurons: Evidence for Four Subtypes of GABAergic Cells in the Inferior Colliculus. *J Neurosci* 36: 3988–3999, 2016. doi:10.1523/JNEUROSCI.0217-16.2016.
- Caspari F, Baumann VJ, Garcia-Pino E, Koch U. Heterogeneity of intrinsic and synaptic properties of neurons in the ventral and dorsal parts of the ventral nucleus of the lateral lemniscus. *Front Neural Circuits* 9: 74, 2015. doi:10.3389/fncir.2015.00074.
- Funahashi M, Mitoh Y, Kohjitani A, Matsuo R. Role of the hyperpolarization-activated cation current (I<sub>h</sub>) in pacemaker activity in area postrema neurons of rat brain slices. *J Physiol* 552: 135–148, 2003. doi:10.1113/jphysiol.2003.047191.
- Geis HR, Borst JG. Large GABAergic neurons form a distinct subclass within the mouse dorsal cortex of the inferior colliculus with respect to intrinsic properties, synaptic inputs, sound responses, and projections. *J Comp Neurol* 521: 189–202, 2013. doi:10.1002/cne.23170.
- Grimsley CA, Sanchez JT, Sivaramakrishnan S. Midbrain local circuits shape sound intensity codes. *Front Neural Circuits* 7: 174, 2013. doi:10.3389/fncir.2013.00174.
- Grimsley JMS, Monaghan JJ, Wenstrup JJ. Development of social vocalizations in mice. *PLoS One* 6: e17460, 2011. doi:10.1371/journal.pone.0017460.
- Hassfurth B, Magnusson AK, Grothe B, Koch U. Sensory deprivation regulates the development of the hyperpolarization-activated current in auditory brainstem neurons. *Eur J Neurosci* 30: 1227–1238, 2009. doi:10.1111/j.1460-9568.2009.06925.x.
- Hurley LM, Tracy JA, Bohorquez A. Serotonin 1B receptor modulates frequency response curves and spectral integration in the inferior colliculus by reducing GABAergic inhibition. *J Neurophysiol* 100: 1656–1667, 2008. doi:10.1152/jn.90536.2008.
- Indig FE, Diaz-Gonzalez F, Ginsberg MH. Analysis of the tetraspanin CD9-integrin alphaIIb beta3 (GPIIb-IIIa) complex in platelet membranes and transfected cells. *Biochem J* 327: 291–298, 1997. doi:10.1042/bj3270291.
- Ito T, Bishop DC, Oliver DL. Two classes of GABAergic neurons in the inferior colliculus. *J Neurosci* 29: 13860–13869, 2009. doi:10.1523/JNEUROSCI.3454-09.2009.
- Ito T, Bishop DC, Oliver DL. Expression of glutamate and inhibitory amino acid vesicular transporters in the rodent auditory brainstem. *J Comp Neurol* 519: 316–340, 2011. doi:10.1002/cne.22521.
- Ito T, Bishop DC, Oliver DL. Functional organization of the local circuit in the inferior colliculus. *Anat Sci Int* 91: 22–34, 2016. doi:10.1007/s12565-015-0308-8.
- Ito T, Oliver DL. Origins of glutamatergic terminals in the inferior colliculus identified by retrograde transport and expression of VGLUT1 and VGLUT2 genes. *Front Neuroanat* 4: 135, 2010. doi:10.3389/fnana.2010.00135.
- Khurana S, Liu Z, Lewis AS, Rosa K, Chetkovich D, Golding NL. An essential role for modulation of hyperpolarization-activated current in the development of binaural temporal precision. *J Neurosci* 32: 2814–2823, 2012. doi:10.1523/JNEUROSCI.3882-11.2012.
- Khurana S, Remme MW, Rinzel J, Golding NL. Dynamic interaction of I<sub>h</sub> and IK-LVA during trains of synaptic potentials in principal neurons of the medial superior olive. *J Neurosci* 31: 8936–8947, 2011. doi:10.1523/JNEUROSCI.1079-11.2011.
- Ko KW, Rasband MN, Meseguer V, Kramer RH, Golding NL. Serotonin modulates spike probability in the axon initial segment through HCN channels. *Nat Neurosci* 19: 826–834; advance online publication, 2016. doi:10.1038/nn.4293.
- Koch U, Braun M, Kapfer C, Grothe B. Distribution of HCN1 and HCN2 in rat auditory brainstem nuclei. *Eur J Neurosci* 20: 79–91, 2004. doi:10.1111/j.0953-816X.2004.03456.x.
- Koch U, Grothe B. Hyperpolarization-activated current (I<sub>h</sub>) in the inferior colliculus: distribution and contribution to temporal processing. *J Neurophysiol* 90: 3679–3687, 2003. doi:10.1152/jn.00375.2003.
- Leao KE, Leao RN, Sun H, Fyffe RE, Walmsley B. Hyperpolarization-activated currents are differentially expressed in mice brainstem auditory nuclei. *J Physiol* 576: 849–864, 2006. doi:10.1113/jphysiol.2006.114702.
- Magnusson AK, Kapfer C, Grothe B, Koch U. Maturation of glycinergic inhibition in the gerbil medial superior olive after hearing onset. *J Physiol* 568: 497–512, 2005. doi:10.1113/jphysiol.2005.094763.
- Merchán M, Aguilar LA, Lopez-Poveda EA, Malmierca MS. The inferior colliculus of the rat: quantitative immunocytochemical study of GABA and glycine. *Neuroscience* 136: 907–925, 2005. doi:10.1016/j.neuroscience.2004.12.030.
- Nagtegaal AP, Borst JG. In vivo dynamic clamp study of I<sub>h</sub> in the mouse inferior colliculus. *J Neurophysiol* 104: 940–948, 2010. doi:10.1152/jn.00264.2010.
- Notomi T, Shigemoto R. Immunohistochemical localization of I<sub>h</sub> channel subunits, HCN1–4, in the rat brain. *J Comp Neurol* 471: 241–276, 2004. doi:10.1002/cne.11039.
- Oertel D. The role of timing in the brain stem auditory nuclei of vertebrates. *Annu Rev Physiol* 61: 497–519, 1999. doi:10.1146/annurev.physiol.61.1.497.

- Oliver DL.** Ascending efferent projections of the superior olivary complex. *Microsc Res Tech* 51: 355–363, 2000. doi:10.1002/1097-0029(20001115)51:4<355:AID-JEMT5>3.0.CO;2-J.
- Ono M, Bishop DC, Oliver DL.** Long-lasting sound-evoked afterdischarge in the auditory midbrain. *Sci Rep* 6: 20757, 2016. doi:10.1038/srep20757.
- Ono M, Bishop DC, Oliver DL.** Identified GABAergic and glutamatergic neurons in the mouse inferior colliculus share similar response properties. *J Neurosci* 37: 8952–8964, 2017. doi:10.1523/JNEUROSCI.0745-17.2017.
- Ono M, Yanagawa Y, Koyano K.** GABAergic neurons in inferior colliculus of the GAD67-GFP knock-in mouse: electrophysiological and morphological properties. *Neurosci Res* 51: 475–492, 2005. doi:10.1016/j.neures.2004.12.019.
- Paxinos G, Franklin K.** *Paxinos and Franklin's the Mouse Brain in Stereotaxic Coordinates* (4th ed.). New York: Academic, 2012.
- Rosenberger MH, Fremouw T, Casseday JH, Covey E.** Expression of the Kv1.1 ion channel subunit in the auditory brainstem of the big brown bat, *Eptesicus fuscus*. *J Comp Neurol* 462: 101–120, 2003. doi:10.1002/cne.10713.
- Scott LL, Mathews PJ, Golding NL.** Posthearing developmental refinement of temporal processing in principal neurons of the medial superior olive. *J Neurosci* 25: 7887–7895, 2005. doi:10.1523/JNEUROSCI.1016-05.2005.
- Shah MM.** Neuronal HCN channel function and plasticity. *Curr Opin Physiol* 2: 92–97, 2018. doi:10.1016/j.cophys.2018.01.001.
- Sturm J, Nguyen T, Kandler K.** Development of intrinsic connectivity in the central nucleus of the mouse inferior colliculus. *J Neurosci* 34: 15032–15046, 2014. doi:10.1523/JNEUROSCI.2276-14.2014.
- Tan ML, Theeuwes HP, Feenstra L, Borst JG.** Membrane properties and firing patterns of inferior colliculus neurons: an in vivo patch-clamp study in rodents. *J Neurophysiol* 98: 443–453, 2007. doi:10.1152/jn.01273.2006.
- Tremblay R, Lee S, Rudy B.** GABAergic interneurons in the neocortex: from cellular properties to circuits. *Neuron* 91: 260–292, 2016. doi:10.1016/j.neuron.2016.06.033.
- Vale C, Sanes DH.** The effect of bilateral deafness on excitatory and inhibitory synaptic strength in the inferior colliculus. *Eur J Neurosci* 16: 2394–2404, 2002. doi:10.1046/j.1460-9568.2002.02302.x.
- Viscomi C, Altomare C, Bucchi A, Camatini E, Baruscotti M, Moroni A, DiFrancesco D.** C terminus-mediated control of voltage and cAMP gating of hyperpolarization-activated cyclic nucleotide-gated channels. *J Biol Chem* 276: 29930–29934, 2001. doi:10.1074/jbc.M103971200.
- Wahl-Schott C, Biel M.** HCN channels: structure, cellular regulation and physiological function. *Cell Mol Life Sci* 66: 470–494, 2009. doi:10.1007/s00018-008-8525-0.
- Walcher J, Hassfurth B, Grothe B, Koch U.** Comparative posthearing development of inhibitory inputs to the lateral superior olive in gerbils and mice. *J Neurophysiol* 106: 1443–1453, 2011. doi:10.1152/jn.01087.2010.
- Xie R, Manis PB.** GABAergic and glycinergic inhibitory synaptic transmission in the ventral cochlear nucleus studied in VGAT channelrhodopsin-2 mice. *Front Neural Circuits* 8: 84, 2014. doi:10.3389/fncir.2014.00084.
- Zhao S, Ting JT, Atallah HE, Qiu L, Tan J, Gloss B, Augustine GJ, Deisseroth K, Luo M, Graybiel AM, Feng G.** Cell-type specific optogenetic mice for dissecting neural circuitry function. *Nat Methods* 8: 745–752, 2011. doi:10.1038/nmeth.1668.

